Fluorescence Resonance Energy Transfer analysis of the structure of the four-way DNA junction

ARTICLE *in* BIOCHEMISTRY · JUNE 1992

Impact Factor: 3.02 · DOI: 10.1021/bi00135a016 · Source: PubMed

6 AUTHORS, INCLUDING:

Robert M Clegg
University of Illinois, Urbana-Champaign
103 PUBLICATIONS **4,747** CITATIONS
SEE PROFILE

Carsten Carlberg
University of Eastern Finland
236 PUBLICATIONS **8,429** CITATIONS
SEE PROFILE

Mergny, J.-L., Sun, J.-S., Rougee, M., Montenay-Garestier, T., Barcelo, F., Chomilier, J., & Hélène, C. (1991) *Biochemistry 30*, 9791-9798.
Mirkin, S. M., Lyamichev, V. I., Drushlyak, K. N., Dobrynin, V. N., Filippov, S. A., & Frank-Kamenetskii, M. D. (1987) *Nature 330*, 495-497.
Mooren, M. M. W., Pulleyblank, D. E., Wijmenga, S. S., Blommers, M. J. J., & Hilbers, C. W. (1990) *Nucleic Acids Res. 18*, 6523-6529.
Parniewski, P., Kwinkowski, M., Wilk, A., & Klysik, J. (1990) *Nucleic Acids Res. 18*, 605-611.
Perrouault, L., Asseline, U., Rivalle, C., Thuong, N. T., Bisagni, E., Giovannangeli, C., Le Doan, T., & Hélène, C. (1990) *Nature 344*, 358-360.
Pilch, D. S., Levenson, C., & Shafer, R. H. (1990) *Proc. Natl. Acad. Sci. U.S.A. 87*, 1942-1946.
Radhakrishnan, I., Gao, X., de los Santos, C., Live, D., & Patel, D. J. (1991) *Biochemistry 30*, 9022-9030.
Radhakrishnan, I., Patel, D. J., & Gao, X. (1992) *Biochemistry 31*, 2514-2523.
Rajagopal, P., & Feigon, J. (1989a) *Nature 339*, 637-640.
Rajagopal, P., & Feigon, J. (1989b) *Biochemistry 28*, 7859-7870.
Roberts, R. W., & Crothers, D. M. (1991) *Proc. Natl. Acad. Sci. U.S.A. 88*, 9397-9401.
Sklenář, V., & Bax, A. (1987) *J. Magn. Reson. 74*, 469-479.
Sklenář, V., & Feigon, J. (1990a) *Nature 345*, 836-838.
Sklenář, V., & Feigon, J. (1990b) *J. Am. Chem. Soc. 112*, 5644-5645.
States, D. J., Haberkorn, R. A., & Ruben, D. J. (1982) *J. Magn. Reson. 48*, 286-292.
Strobel, S. A., & Dervan, P. B. (1991) *Nature 350*, 172-174.
Strobel, S. A., Moser, H. E., & Dervan, P. B. (1988) *J. Am. Chem. Soc. 110*, 7927-7929.
Weinreb, A., Collier, D. A., Birshtein, B. K., & Wells, R. D. (1990) *J. Biol. Chem. 265*, 1352-1359.
Wells, R. D., Collier, D. A., Hanvey, J. C., Shimizu, M., & Wohlrab, F. (1988) *FASEB J. 2*, 2939-2949.
Wüthrich, K. (1986) *NMR of Proteins and Nucleic Acids*, John Wiley & Sons, Inc., New York.

Fluorescence Resonance Energy Transfer Analysis of the Structure of the Four-Way DNA Junction†

Robert M. Clegg,*,‡ Alastair I. H. Murchie,§ Annelies Zechel,‡ Carsten Carlberg,‡ Stephan Diekmann,‡ and David M. J. Lilley§

Department of Molecular Biology, Max Planck Institute for Biophysical Chemistry, Postfach 2841, D-W-3400 Göttingen, Federal Republic of Germany, and Department of Biochemistry, The University, Dundee DD1 4HN, U.K.

Received May 14, 1991; Revised Manuscript Received December 9, 1991

ABSTRACT: We have carried out fluorescence resonance energy transfer (FRET) measurements on four-way DNA junctions in order to analyze the global structure and its dependence on the concentration of several types of ions. A knowledge of the structure and its sensitivity to the solution environment is important for a full understanding of recombination events in DNA. The stereochemical arrangement of the four DNA helices that make up the four-way junction was established by a global comparison of the efficiency of FRET between donor and acceptor molecules attached pairwise in all possible permutations to the 5′ termini of the duplex arms of the four-way structure. The conclusions are based upon a comparison between a series of many identical DNA molecules which have been labeled on different positions, rather than a determination of a few absolute distances. Details of the FRET analysis are presented; features of the analysis with particular relevance to DNA structures are emphasized. Three methods were employed to determine the efficiency of FRET: (1) enhancement of the acceptor fluorescence, (2) decrease of the donor quantum yield, and (3) shortening of the donor fluorescence lifetime. The FRET results indicate that the arms of the four-way junction are arranged in an antiparallel stacked X-structure when salt is added to the solution. The ion-related conformational change upon addition of salt to a solution originally at low ionic strength progresses in a continuous noncooperative manner as the ionic strength of the solution increases. The mode of ion interaction at the strand exchange site of the junction is discussed.

Recombination between DNA molecules is of great biological importance. Homologous recombination in chromosomes of diploid organisms generates reassortment of genes that allows the best combinations to be selected and is thus of enormous significance in evolution. Site-specific recombination systems are involved in many DNA rearrangements from the integration of bacteriophage genomes to the generation of antibody diversity.

Most models for homologous genetic recombination postulate a four-way (Holliday) junction in DNA as the central intermediate (Holliday, 1964; Meselson & Radding, 1975; Orr-Weaver et al., 1981) that must undergo subsequent cleavage (resolution) to recreate unconnected duplex molecules. Early attempts to model the molecular geometry (Calascibetta et al., 1984; Sigal & Alberts, 1972; Sobell, 1972) all involved

† We are indebted to NATO for a travel grant and the Wellcome Trust and the C.R.C. for financial support.
* Author to whom correspondence should be addressed.
‡ Max Planck Institute for Biophysical Chemistry.
§ The University, Dundee.

0006-2960/92/0431-4846$03.00/0

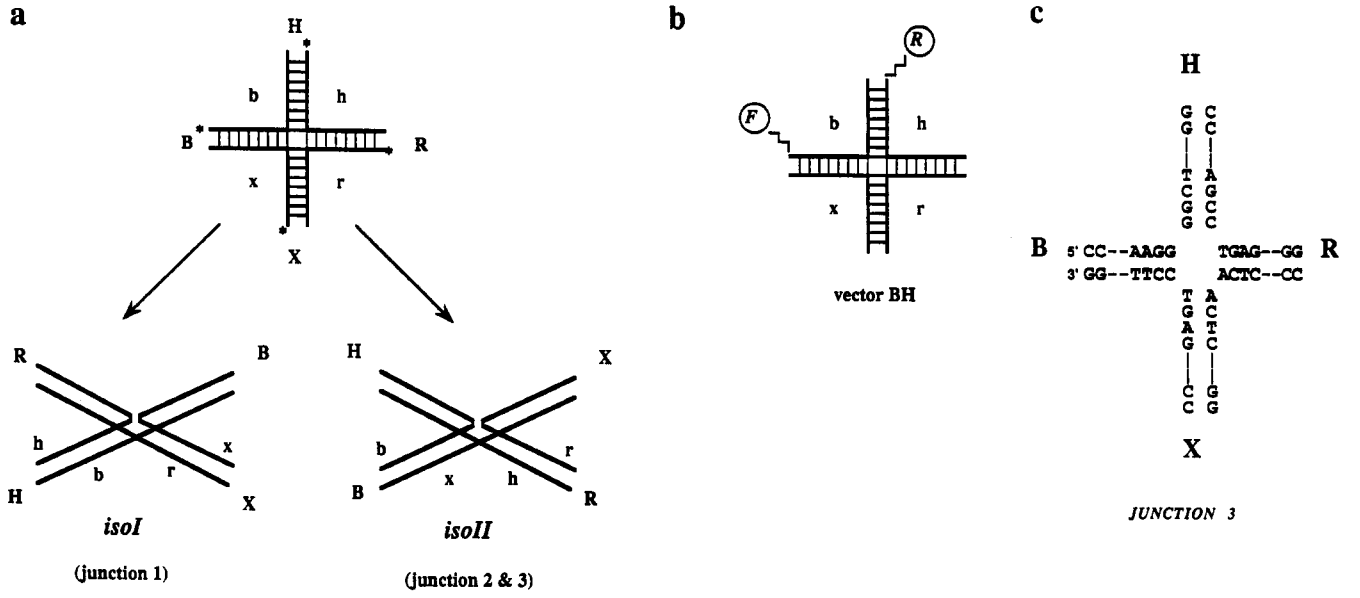

FIGURE 1: Proposed folding of the four-way DNA junction into a stacked X-structure (Duckett et al., 1988; Murchie et al., 1989; von Kitzing et al., 1990). (a) Schematic of the folding pattern of the four-way junction. Our DNA junctions are constructed from four single-stranded oligonucleotides, b, h, r, and x, that are hybridized together to generate the four duplex arms of the junction B, H, R, and X as shown. Asterisks denote 5′ termini. Gel electrophoresis and FRET experiments have indicated that, on addition of magnesium or other cations, the junction undergoes a folding into an X-shaped structure, in which there is end-on-end helix–helix stacking to generate two coaxial helical stacks. Two isomers of the structure are possible, which differ in the nature of the stacking partners. In the iso I conformation the B arm is stacked with the H arm, while in the iso II conformation the B and X arms are stacked. (b) The energy transfer experiments are carried out on junctions comprising four 34 nt oligonucleotides. The junctions are assembled from one oligonucleotide with a fluorescein fluorophore attached via a C6 linker at the 5′ terminus, one oligonucleotide with an equivalently attached rhodamine dye, and two unconjugated oligonucleotides. The result is a junction with fluorescein and rhodamine dyes attached to the termini of different arms. There are six possible end-to-end vectors that can be labeled this way in either direction (e.g., B-fluorescein and H-rhodamine or B-rhodamine and H-fluorescein; in our nomenclature, followed throughout this paper, these vectors are referred to as BH and HB respectively, i.e., the vector is in the direction of donor–acceptor). (c) The central sequence of junction 3. The sequence around the point of strand exchange is identical to that of the junction 3 used in previous gel electrophoresis experiments (Duckett et al., 1988). Each of the 17 bp arms terminate in a 5′-CC sequence in order to keep any interactions between the dyes and the DNA constant.

association of helical arms in pairs by means of stacking. The majority of models have placed the resulting quasicontinuous helices side-by-side, with a parallel alignment, and indeed this is the most frequent representation in textbook models of recombination. We have proposed a working model for the structure of the four-way DNA junction, termed the stacked X-structure, based upon experimental and stereochemical considerations (Duckett et al., 1988; Murchie et al., 1989; von Kitzing et al., 1990). In the presence of sufficient cations, the junction undergoes pairwise stacking of helical arms, to generate two quasicontinuous, coaxial helices (Figure 1a) that are in the form of a right-handed X-shape. The 2-fold symmetry of the structure generates two different kinds of strand; continuous strands pass essentially undeviated along the length of the coaxial helices, while the exchanging strands pass between the two coaxial helices at the point of strand exchange, i.e., the junction itself. In the proposed structure, the exchanging strands are disposed across the small angle of the X, i.e., there is an approximately antiparallel alignment of the continuous strands.

The antiparallel X-structure is consistent with the results of gel electrophoresis (Cooper & Hagerman, 1987; Duckett et al., 1988; Gough & Lilley, 1985), fluorescence resonance energy transfer (FRET) experiments (Murchie et al., 1989), electric birefringence measurements (Cooper & Hagerman, 1989), and magnetic birefringence and neutron scattering experiments (J. Torbet, A. I. H. Murchie, and D. M. J. Lilley, unpublished observations). The 2-fold symmetry of the structure is also in agreement with experiments in which junctions were probed with hydroxyl radicals (Churchill et al., 1988). An approximate colinearity of the stacked helical arms was indicated by the ability of the restriction enzyme *Mbo*II to cleave across the junction (Murchie et al., 1991). In the right-handed, antiparallel structure, the continuous strands are accommodated in the major grooves of the opposed helices (Murchie et al., 1989; von Kitzing et al., 1990); this interaction is optimal for a small angle of 60°. A similar arrangement has been observed in a crystal structure of a piece of double-stranded DNA (Timsit et al., 1989), and this alignment of strands and grooves is consistent with the protection that the structure affords to the DNA against cleavage by DNase I (Lu et al., 1989; Murchie et al., 1990).

Two isomers of the proposed right-handed antiparallel stacked X-structure are possible, depending on the choice of stacking partners (Figure 1a). Our original gel electrophoresis experiments suggested that two of the original four-way junctions that we constructed, junctions 1 and 2, represented the two different isomeric conformations, iso I (H arm stacked on B) and iso II (B stacked on X), respectively, and that junction 3 adopted the iso II conformation (i.e., comparable to junction 2). FRET experiments (Murchie et al., 1989) were fully consistent with the iso I and iso II conformations of junctions 1 and 2, respectively.

In the absence of added metal ions, we observed marked differences in the gel electrophoretic migration of junctions, obtaining results clearly suggesting a square configuration of arms (Duckett et al., 1988). The extended structure suggested was consistent with the reactivity of thymine bases at the point of strand exchange at low salt concentration (Duckett et al., 1988, 1990).

In this study, we have employed FRET to study the configuration of helical arms in a particular four-way junction and the variation of conformation with environmental conditions. This technique exploits the coupling between the

transition dipoles of two different fluorophores attached to a macromolecule to derive distance information over a range of 20–80 Å. We have synthesized a complete series of synthetic four-way junctions with donor and acceptor fluorophorent dyes conjugated to the 5′ termini of the different pairs of the helical arms of the four-way junction. A global comparison of the efficiency of FRET measurements on these molecules provides evidence to deduce which alternative structures predominate in different solution conditions. The FRET data on a new junction sequence (junction 3; the central sequence is given in Figure 1c) are in good agreement with our deductions from gel electrophoresis (Duckett et al., 1988) and earlier FRET (Murchie et al., 1989) experiments. In these studies, we have employed three FRET techniques to the study of nucleic acid solution conformation: (1) enhanced emission of the acceptor (rhodamine), (2) decrease in the fluorescence quantum yield of the donor (fluorescein), and (3) decrease in the excited state lifetime of the donor. The response of the four-way junction to Mg^{2+}, Ca^{2+}, and Na^{+} cations, and the apparent affinities, has been determined from ion titrations by observing fluorescence energy transfer. From these studies, we are able to discuss the probable mode of binding by these ions to the DNA junction, and the role of cations in the folding process.

Materials and Methods

Synthesis and Purification of Oligonucleotides. Oligonucleotides were synthesized using β-cyanoethylphosphoramidite chemistry (Beaucage & Caruthers, 1981; Sinha et al., 1984) implemented on 381A and 394 DNA synthesizers (Applied Biosystems). 5′-Amino groups at the end of six-carbon linkers were introduced by means of a final coupling step with *N*-methoxytrityl-2-aminohexyl-2-cyanoethyl-*N*,*N*-diisopropylamino phosphite (Connolly, 1987) (BDH). Fully deprotected oligonucleotides were ethanol precipitated and purified by HPLC on a 4000A DEAE weak anion exchange column (Nucleogen), followed by a C8 reverse-phase column (Aquapore). Pure oligonucleotides eluted as sharp peaks. Peak fractions were reduced in volume and ethanol precipitated.

Conjugation with Fluorescent Dyes. One A_{258} unit of each oligonucleotide was reacted with 10 mg/mL of the *N*-hydroxysuccinamide ester of tetramethylrhodamine (Molecular Probes) in dimethyl sulfoxide with 0.2 M carbonate buffer, pH 9.5. Oligonucleotides were conjugated with fluorescein by reaction with 1.5 mg/mL fluoresceinisothiocyanate (Molecular Probes) in dimethylformamide with 0.3 M carbonate buffer, pH 9.5. Unreacted dyes were removed by chromatography on Sephadex G25 (Pharmacia). Dye-conjugated and unreacted oligonucleotides were separated by electrophoresis in 20% polyacrylamide in 90 mM Tris borate, pH 8.3, 7 M urea. The conjugated oligonucleotides migrated as single fluorescent bands that were retarded by more than the equivalent of one nucleotide relative to the unreacted species. These were excised, and DNA was recovered by electroelution and ethanol precipitation. This method was designed to yield 100% labeled DNA, and this was confirmed spectroscopically.

Construction of Fluorescently Labeled Four-Way Junctions. It is essential to purify all four-way junction species by gel electrophoresis, in order to ensure the complete removal of nonstoichiometric contaminants. Suitable combinations of the labeled and unconjugated oligonucleotides (0.04 A_{258} units) were hybridized in 450 mM NaCl, 24 mM sodium citrate, pH 7.0, and 2 mM $MgCl_2$ by slow cooling from 65 to 10 °C. Junctions were purified by electrophoresis in 8% polyacrylamide gels in 90 mM Tris·borate, pH 8.3, and 2 mM $MgCl_2$ with circulation of the buffer. The junction species were significantly retarded relative to the single strands and two- and three-arm species. Bands containing four-way junctions were electroeluted, and the resulting DNA was ethanol precipitated. The extent of labeling was verified by absorption measurements at 260, 496, and 558 nm; absorption spectra are not as sensitive to the conjugation or the molecular environment as fluorescence spectra.

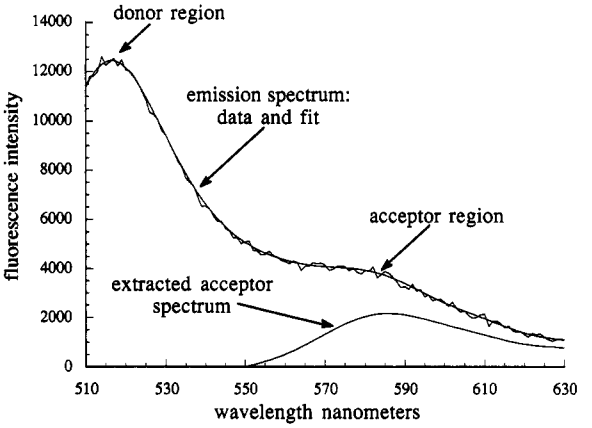

FIGURE 2: Example of FRET data analysis; measurement of enhanced acceptor emission of a doubly labeled junction. The emission spectrum is excited at 490 nm; the fitted spectrum is also shown. Between 500 and 530 nm, only fluorescein fluoresces; rhodamine has maximum emission at 585 nm. The "extracted acceptor emission" $F^{A}_{em}(\nu,\nu')$ is obtained by fitting the original spectrum to a standard fluorescein spectrum (conjugated with fluorescein to a junction with identical nucleotides at the end of the labeled arm) between 510 and 530 nm. The fluorescein (donor) contribution is then subtracted from the FRET data, giving the pure acceptor spectrum shown in the figure. An excitation spectrum, $F^{A}_{ex}(\nu,\nu'')$, of the same sample is taken from 400 to 590 nm, with emission in the range of 580–600 nm. This excitation spectrum is fitted with polynomials similarly to the emission spectrum, and the peak [$\lambda_{max} \sim 565$ nm of $F^{A}_{ex}(\nu_2,\nu'')$ where only rhodamine absorbs] is divided into the derived acceptor emission spectrum of this figure. The buffer signal, which contains the Raman emission from water, is subtracted from every fluorescence spectrum.

Preparation of the Probes for Fluorescence and Absorption Experiments. All labeled junction samples were spun down in ethanol solution, dried under vacuum, and dissolved into the fluorescence buffer (90 mM Tris·borate, pH 8.3). Absorption measurements were made on these solutions, from 230 to 600 nm; these spectra were used to determine the concentration of the junctions (DNA and the probes) and in conjunction with the fluorescence measurements (Figure 2) determined the consistency of the labeling efficiency. All samples were measured at 20 °C. The junction 3 probes were first dissolved in the buffer without salt, and the absorption and fluorescence measurements were then performed. For the series of junction measurements on junction 3, the salt was added from a concentrated Mg^{2+} solution in one step.

The ion titrations were measured on samples starting with low salt and 20 μM EDTA to ensure that divalent metals were removed from solution. The different ionic solutions ($MgCl_2$, $CaCl_2$, and NaCl) were added sequentially from concentrated stock salt solutions; steady-state fluorescence measurements were made within 10 min after each salt addition. The nanosecond lifetime measurements were made after completing the steady-state measurements to minimize photolysis of fluorescein.

Description of the Spectroscopy Equipment, Steady-State, and Time-Resolved. Absorption measurements were taken on either a Uvicon 820 (Kontron) or a Cecil CE6600 spectrophotometer. All steady-state fluorescence experiments were made with a SLM 8000S (Urbana, IL) instrument. Excitation and emission spectra were corrected for lamp fluctuations and wavelength variations. Polarization artifacts were avoided by

employing "magic angle" conditions (Nickel, 1989). Excitation and emission fluorescence spectra were fitted to a series of Chebyshev polynomials (De Boeck et al., 1985). Spectra for FRET were collected over a broad range of excitation and emission wavelengths (excitation spectra, λ_{ex} = 400–590 nm, λ_{em} = 600 nm; emission spectra, λ_{ex} = 490 nm, λ_{em} = 500–650 nm). The absorption of all solutions used for the fluorescence measurements at the wavelength of excitation was always below 0.015. The fluorescence spectra of junctions singly labeled with fluorescein and rhodamine were used to decompose the doubly labeled fluorescence spectra into donor and acceptor components.

Nanosecond lifetime measurements were carried out with the method of phase and modulation (Gratton & Limkeman, 1983; Spencer & Weber, 1969), and the instrument has been described recently (Piston et al., 1989). A rotating thermostated cuvette holder has been implemented to allow the simultaneous measurement of three samples and one reference, all with separate filter combinations. The reproducibility of the measurements within a series of measurements was ~100 ps. This was sufficient to detect differences of 200–500 ps needed to distinguish the various labeled isomers. The data were analyzed with a software package from Globals Unlimited (Laboratory for Fluorescence Dynamics, Urbana, IL). The decay of fluorescein emission was selected, exciting with the 476.5- or 488-nm line of a 2035 Spectra Physics argon ion laser and observing the fluorescence through a 520 narrow band-pass filter (520 SS, Corion, band-pass = 10 nm). All samples were measured at least twice. About 80% of the decay amplitude was assigned to a slower component of 2.6–3.2 ns. The shorter times of the faster decay process, 300–600 ps, approach the limit of our instrument. Magic angle positions of the excitation and emission polarizers were employed to eliminate polarization artifacts. The temperature was 20 °C.

The appendix summarizes the theory and data analysis of the FRET measurements which are used to analyze the fluorescence experiments and the ion titrations.

Results

Extent of Labeling in the Dye-Conjugated Four-Way Junctions. In these investigations, we have studied the interaction between donor (fluorescein) and acceptor (rhodamine) fluorophores attached to the 5′ ends of different arms of a four-way DNA junction. As explained in Figure 1, there are six possible end-to-end vectors that can be studied by this technique, comparison of which allows structural models for the junction to be tested under a variety of solution conditions.

The procedures used to prepare the labeled junctions were designed to ensure virtually 100% labeling of the DNA molecules with the dyes. After conjugation of the single strands with fluorescein or rhodamine, they were electrophoresed in polyacrylamide. The conjugated and unconjugated DNA are significantly separated by this technique. The conjugated DNA could readily be purified by excision of the band and electroelution of the DNA. Following hybridization of the four strands, the DNA was electrophoresed in polyacrylamide and pure four-way junction recovered by electroelution.

Absorption and Fluorescence Spectra Testify to the Integrity of the Junctions and Their Suitability for Energy Transfer Measurements. We confirmed spectroscopically that the dyes were equimolar. The visible absorption bands (450–600 nm) are well removed from the UV absorption of the DNA (260 nm). The acceptor absorption at its maximum (λ = 558 nm) can be measured without interference from the donor. With knowledge of the acceptor absorbance spectrum, the overlapping contribution by the acceptor can be subtracted from the total absorbance spectrum, yielding the true donor absorbance at the wavelength of maximum donor absorption (λ = 496 nm). A linear relation that intercepts the ordinate at the origin is obtained by plotting pairs of absorption maxima of DNA, fluorescein, and rhodamine (at 260, 496, and 558 nm) within the series of probes (data not shown). Such relative absorption measurements show that the extents of labeling of both dyes were constant for all the experiments. The experimentally determined coefficient of variance of the ratio of rhodamine to fluorescein labeling was 0.8%; the major source of error is the absorption measurement, due to low concentrations. The absorbance and fluorescence spectral shapes of all labeled junctions are identical, indicating that the environment of the dyes in all junctions is very similar. This is expected since precautions have been taken to keep the two terminal base pairs of every helix the same.

The absorption coefficients (ϵ's) of 100% conjugated dyes can be calculated from the labeled junctions knowing the absorption values of different areas of the spectrum of the DNA and the two conjugated dyes. Using ϵ_{DNA} (258 nm) = 13 820 M^{-1} cm^{-1} per base pair (estimated from the GC and AT %) gives $\epsilon_{fluorescein}$ = 46 000 M^{-1} cm^{-1} and $\epsilon_{rhodamine}$ = 75 200 M^{-1} cm^{-1}. $\epsilon_{rhodamine}$ is not significantly affected by conjugation to the oligomers; however, the $\epsilon_{fluorescein}$ has been decreased by about one-third compared to the values found for the free dye, in good agreement with previous findings that conjugation of fluorescein to macromolecules considerably decreases its absorption coefficient [Haugland (1989) and Molecular Probes catalogue (1989) Eugene, OR].

Anisotropy Measurements Indicate That the Fluorescein Is Very Mobile. Fluorescence measurements at λ_{ex} = 490 nm and λ_{em} = 514 nm detect only fluorescein; λ_{ex} = 565 nm and λ_{em} = 600 nm detects only rhodamine; therefore, the fluorescence anisotropy of each fluorescence probe can be measured independently, even in the doubly labeled junctions. Rhodamine conjugated to the junctions has an anisotropy of 0.25, essentially independent of the ionic strength. The anisotropy of the fluorescein fluorescence is 0.07 at low salt concentrations and 0.11 at the higher salt concentrations (singly labeled junctions). Because the fluorescence lifetimes of both dyes are similar and they are attached to the same macromolecule, fluorescein must undergo considerably faster rotational diffusion, or rotate rapidly within a greater cone angle, than rhodamine (the maximum anisotropy possible for both dyes is almost 0.4). Rapid movements of dyes within their excited state lifetime and random static orientations of the dye transition moments simplify the interpretation of energy transfer measurements (Förster, 1951; Steinberg, 1968). Because of the low anisotropy of fluorescein, and the lack of indication, or expectation, that fluorescein is located in a preferred static orientation relative to the DNA helix, we assume a random relative orientation of the dyes with rapid reorientational motion with a constant κ^2 value. More important than the actual value of κ^2 is its consistency throughout the series of labeled junction molecules for any particular solution condition. Precautions have been taken to keep the environment of the dyes the same for all molecules.

Steady-State FRET Measurements Register a Conformational Change in the Junction Structure with and without Added Salt. A comparison of the extent of energy transfer for a series of labeled junction 3 molecules with and without added Mg^{2+} is shown in Figure 3 in terms of the acceptor energy transfer ratio, $(ratio)_A$ (see Appendix, eqs A3 and A5). Fluorescence spectra were recorded for the 12 doubly labeled

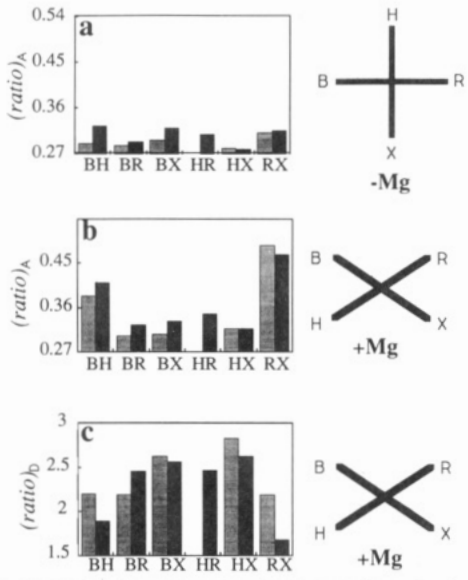

FIGURE 3: Steady-state measurements of energy transfer for junction 3 by means of comparison between different end-to-end vectors. All six vectors in both directions were measured, with the exception of the HR (i.e., H-fluorescein–R-rhodamine) vector. Stick figures to the right of the plots indicate the configuration of the ends of the arms that are globally consistent with the corresponding data. $(ratio)_A$ and $(ratio)_D$ refer to the expressions given in eqs A5 and A6 of the text. (a) Enhancement of acceptor emission in the absence of added magnesium. Plot of $(ratio)_A$ for the series of end-to-end vectors. The reproducibility was 2–4% depending upon the fluorescence magnitudes. (b) Enhancement of acceptor emission in the presence of 5 mM magnesium. Plot of $(ratio)_A$ for the series of end-to-end vectors. The relative values of $(ratio)_A$ remain the same if the salt is added to the low salt samples or if the samples are all dialyzed against the same higher salt buffer. (c) Donor fluorescence in the presence of 5 mM magnesium. Plot of $(ratio)_D$ for the series of end-to-end vectors. Because the Φ^D is strongly dependent upon the ion concentration (see Figure 5), it is essential to dialyze all the samples against the same buffer to ensure that the ion concentrations are the same.

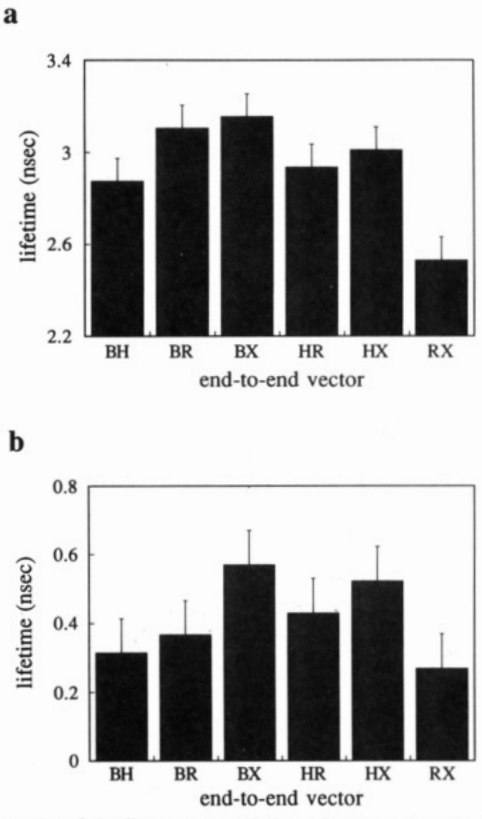

FIGURE 4: Plot of the fluorescence lifetimes for the series of end-to-end vectors of junction 3 (see eq A2). Lifetimes were measured with a sample temperature of 10 °C. As with the $(ratio)_D$ data in Figure 3c, it was necessary to dialyze all the samples against the same buffer to ensure that the ion concentrations were exactly the same. (a) Slower decay times. (b) Faster decay times. The amplitudes of the slower times are ~80% of the total amplitudes. The samples were measured twice; time analyses were reproducible within ~100 ps, shown by the error bars.

species of junction 3 (i.e., six end-to-end vectors, each in either direction). The error in the calculation of $(ratio)_A$ was determined directly by repeating the experiments with analysis many times on a few junctions. The experiments with the variously labeled junction 3 molecules are reproducible within 2–4%, depending upon the fluorescence intensities.

In the absence of added magnesium (Figure 3a), the energy transfer for all six vectors is low [$(ratio)_A$=0.27 for singly labeled rhodamine junctions], consistent with an extended structure. Despite this low extent of FRET, there is an indication that the two vectors BR and HX have the lowest extents of energy transfer. This is consistent with a structure where the ends of the arms are located in the four corners of a square, as has been proposed from electrophoresis experiments (Duckett et al., 1988).

Upon addition of magnesium ions (Figure 3b), the pattern of energy transfer alters significantly. Under these conditions, the FRET for the vectors BH and RX is considerably enhanced. This is consistent with the stacked X-structure iso II, in which the B and X arms are stacked, as are the H and R arms, with an acute angle between B and H, and X and R (refer to Figure 1).

FRET was also measured from the decrease in the steady-state donor fluorescence (Figure 3c; eq A6). These samples were dialyzed against the same buffer solution to ensure that each solution has the same ionic conditions and therefore the same Φ^D. Both spectra for the numerator and denominator of eq A6 were taken as excitation spectra. The wavelengths were $\lambda' = 490$ nm, $\lambda'' = 560$ nm, $\lambda_1 = 518$ nm, and $\lambda_2 = 600$ nm, according to the superscript and subscript labeling given for eq A6. Figure 3c shows that the samples which show the maximum enhanced acceptor fluorescence signal have the least donor fluorescence.

The Steady-State Fluorescence Measurements Have Been Extended by Nanosecond Lifetime Measurements. Nanosecond lifetimes of the same samples as in Figure 3 are plotted in Figure 4. The data have been fitted to two lifetimes; both lifetimes behave similarly within the series of measurements. The singly labeled fluorescein samples also show two times. Fitting three times does not improve the goodness of the fit. Those samples which according to the two steady-state FRET methods show the highest efficiency of energy transfer have the lowest lifetimes; therefore, the results of the two methods support the same structure of the junction. However, since E is low for these junctions, the lifetimes do not vary much, and accurate values of E are difficult to calculate. The existence of multiple lifetimes complicates a quantitative FRET analysis. One might expect at least two emitting fluorescein species and a distribution of D–A distances. However, a qualitative evaluation of the FRET data, which requires only that E is larger for smaller distances, can still be made.

The Progress of the Folding Reaction May Be Followed by Energy Transfer as the Concentration of Ions (NaCl, $MgCl_2$, and $CaCl_2$) Increases. For these experiments, junction 1 molecules labeled across an acute angle (when folded) were employed. These data for the ion titrations are presented in Figure 5a–f. The fluorescence values of the singly labeled fluorescein junctions are plotted as a function of the $MgCl_2$ and $CaCl_2$ concentration; fluorescein is quenched considerably.

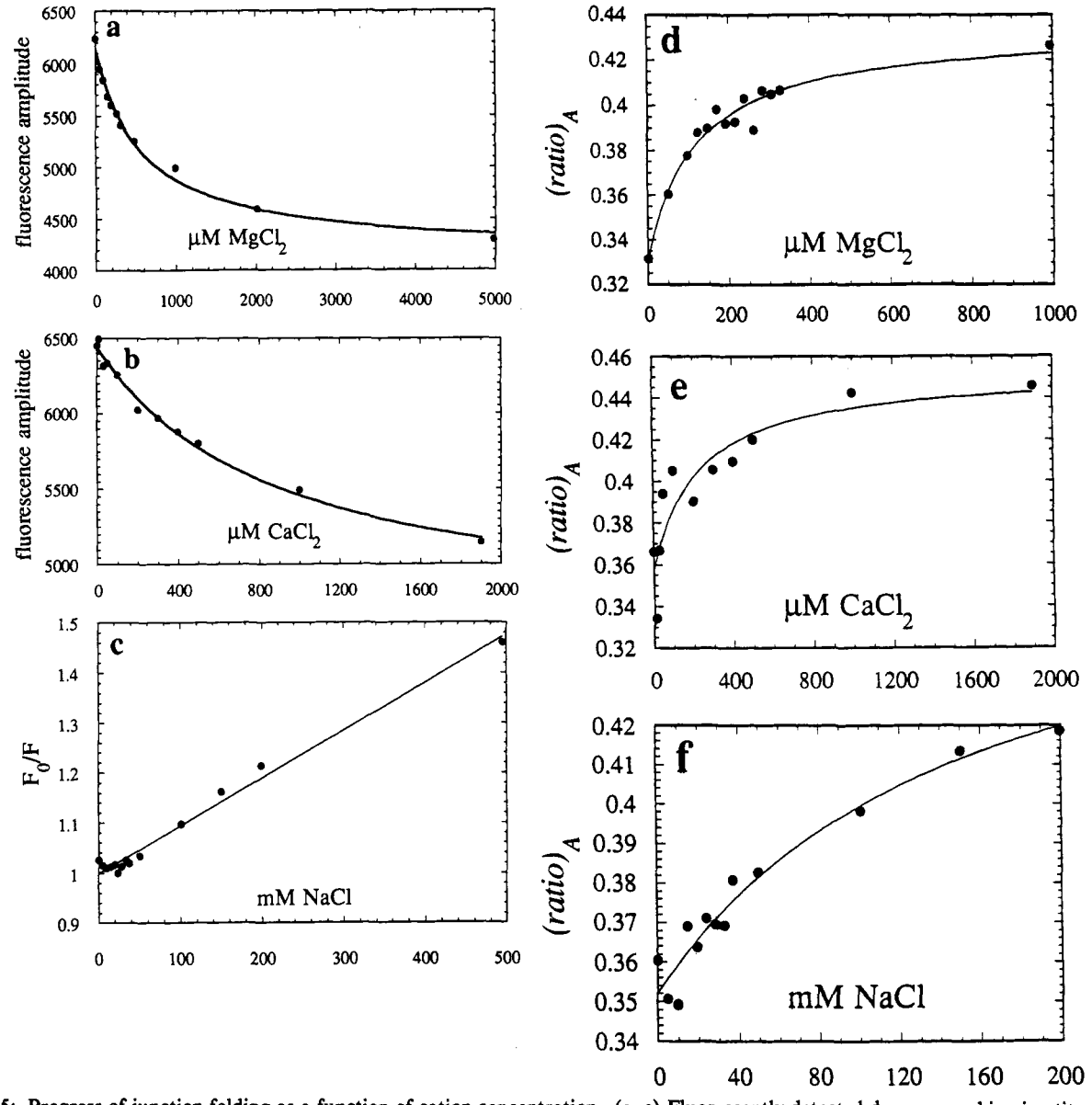

FIGURE 5: Progress of junction folding as a function of cation concentration. (a–c) Fluorescently detected donor quenching ion titrations of junction 1 (singly labeled with fluorescein) samples for $MgCl_2$ (a), $CaCl_2$ (b), and NaCl (c). The NaCl titration is presented as a Stern–Volmer plot (see text). The curves are fits to either a simple bimolecular binding function (a and b), or a straight line (c); the slope in (c) is 0.96 M^{-1}. The parameters of these fits are used to correct for quenching of the donor in the analysis of the following data. (d–f) Ion titrations of junction 1 samples doubly labeled with fluorescein and rhodamine (which according to the X model have the donor and acceptor across an acute angle) for $MgCl_2$ (d), $CaCl_2$ (e), and NaCl (f). $(ratio)_A$ is plotted vs the concentration of added salts. The continuous lines are fits to the data corresponding to the apparent dissociation binding constants, K_{cation}, and correlation coefficients (r) of (d) 120 μM for $MgCl_2$ (r = 0.98), (e) 230 μM for $CaCl_2$ (r = 0.91), and (f) 154 mM for NaCl (r = 0.97).

The fluorescence quenching of a singly labeled fluorescein junction by NaCl can be accounted for by a Stern–Volmer analysis with 100% quenching; the slope of 0.9 M^{-1} (Figure 5c and see Appendix) is lower than expected for a fluorescein molecule that is fully susceptible to collisions from all directions, which would have a slope of ~3–30 M^{-1}. This is expected for dynamic quenching since the approach of the ions will be hindered by the tether and the proximity of the dye to the DNA. This result, together with the linearity of the Stern–Volmer plot, indicates that NaCl (probably the Cl^- ion) quenches fluorescein fluorescence by an unspecific collisional mechanism. In contrast, the interactions of $MgCl_2$ and $CaCl_2$ cannot be due to collisional quenching. Apparently there is an interaction of the Ca^{2+} and Mg^{2+} ions with fluorescein, which has a much higher affinity than Na^+ (the anions are the same for all salts).

The Mg^{2+} and Ca^{2+} titrations of the singly fluorescein labeled junctions (Figure 5a,b) can be analyzed as a simple bimolecular binding reaction; the resulting dissociation constants (K_d) are 0.570 and 0.900 mM for Mg^{2+} and Ca^{2+}, respectively. Mg^{2+} and Ca^{2+} ions quench the fluorescence of the conjugated fluorescein maximally by 32% and 29% (the total concentrations of $MgCl_2$ and $CaCl_2$ are so low that dynamic unspecific quenching is relatively insignificant).

As a consequence of the fluorescein (donor) fluorescence quenching just discussed, R_0 changes as the salt concentration is varied (see sentence following eq A1). However, as discussed in the Appendix, the ion titration curves can be corrected in order to determine effective dissociation binding constants of the doubly labeled junctions (legend to Figure 5). The corrected titration curves are given in Figure 5d–f. It is apparent from these titration curves in Figure 5d–f that the FRET signal accompanying the folding process increases continually over an extended ion concentration range and that the ion-induced junction folding is not a highly cooperative process. In addition, the values of the apparent dissociation constants (120

μM for $MgCl_2$, 230 μM for $CaCl_2$, and 154 mM for NaCl; see Appendix) do not correspond to particularly high affinities of cations for DNA.

Discussion

The Determination of the Global Stereochemistry of the Four-Way Junction Is Based Mainly upon a Comparison of a Series of Energy Transfer Measurements on Identical Junction Molecules with Permuted Labeling Positions, Rather Than upon Solitary Estimates of Donor–Acceptor Distances. We have focused upon determining experimental quantities proportional to the transfer efficiency E (see Appendix). The experiments are designed so that the predominant molecular information can be deduced from accurate comparisons of energy transfer efficiencies within a series of similar molecular species. Our conclusions rest essentially upon the assumption that D–A pairs which are closer together will transfer energy more efficiently than D–A pairs which are farther apart. No other assumption about the functional dependence of E upon R, is required.

The Energy Transfer Measurements Are Consistent with an Antiparallel Stacked X-Structure of the Four-Way Junction in the Presence of Mg^{2+}. Our earlier experiments have led us to propose that the four-way junction is folded into an X-shaped structure in the presence of sufficient cations, each arm of the X representing one of the four helical arms of the junction (Duckett et al., 1988; Murchie et al., 1989; von Kitzing et al., 1990; see Figures 1 and 6 and the introduction). By labeling the junction molecules at the extremities of the arms with a donor and acceptor molecule in all possible permuted positions, and comparing the extent of energy transfer, we can decide whether the X-structure accounts globally for the relative energy transfer.

The steady-state (Figure 3) and the time-resolved energy transfer experiments (Figure 4) on the series of labeled junctions are all in agreement with the prediction from the X-structure that there are two pairs of arm extremities—those bridged by the two acute angles—that are closer than all other pairs of extremities. In addition, these results determine which helices (arms) stack upon one another; there are only two ways of producing two pairs of arms that are closest together, and the choices for stacking in the two cases are mutually exclusive. Thus in order for the short end-to-end vectors of junction 3 to be BH and RX, arm B must stack upon X and H upon R. A ribbon representation of this structure is presented in Figure 6. Note that for the B and H arms to be close, the b strand must define one of the acute angles in the structure; similarly the r strand must define the other. Thus the exchanging strands (b and r) do not formally cross one another, and there is an approximately antiparallel alignment of the continuous strands (h and x) in the structure.

The results with junction 3 agree with the earlier studies of four-way junctions. Gel electrophoresis studies (Duckett et al., 1988) had indicated that three junctions (junction numbers 1, 2, and 3) of related sequence each adopted an X-shaped conformation, consistent with coaxial helix–helix stacking, but that junction 1 had an isomeric conformation (iso I) in which there was H on B stacking, while junctions 2 and 3 adopted the alternative isomeric conformation (iso II) with B on X stacking. Our previous fluorescence energy transfer studies (Murchie et al., 1989) were in agreement with the structures of junctions 1 and 2, and the present study now supports the iso II stacked X-conformation of junction 3; the quasicontinuous helices of junction 2 were found to be rotated in a right-handed sense relative to each other (Murchie et al., 1989). This structure also rationalizes the interaction between

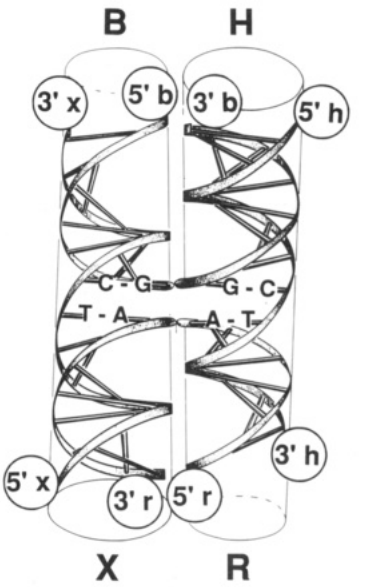

FIGURE 6: Stacked X-structure for junction 3. The structure shown is a ribbon representation of the X-structure that is consistent with all the FRET data for junction 3 in the presence of added cations. The FRET measurements indicate that the shortest end-to-end distances are BH and RX. This is indicated consistently by studies of enhanced steady-state emission, reduced fluorescein steady-state fluorescence, and direct measurements of fluorescence lifetimes of the donor. The right-handed, antiparallel stacked X-structure has been proposed as a working model for the four-way junction on the basis of a variety of experimental data. The FRET data are fully consistent with the iso II form of this structure, in which the B and X arms are stacked to form a coaxial, quasicontinuous helix containing a continuous x strand, and the H and R arms form the other coaxial stack, with a continuous h strand. The polarities of the strands are indicated, along with the bases that define the point of strand exchange.

the four-way junction and resolving enzymes (Bhattacharyya et al., 1991).

The disposition of the helices (antiparallel and angular juxtapositions) is at variance with the usual parallel and side-by-side representation given in textbooks. The important features of the model are (1) both angles between the two pairs of helices each containing one of the exchanging strands are more acute than the other two angles at the junction, and (2) the exchanging DNA strands run in antiparallel directions (that is, fold back more than 90°) on either side of the junction. How flexible the junction is, the degree of straightness of the quasicontinuous helices, and the extent to which the junction has a perfect X-structure, remain questions for more refined solution experiments; fluorescence methods will help provide more details in the future.

Another study of four-way junctions by FRET has been published recently (Cooper & Hagerman, 1990), in which data were obtained that are in agreement with the antiparallel X-shaped structure of the junction in the presence of additional salt. These authors have, nevertheless, questioned the applicability of the FRET technique to analyze nucleic acid structures. Their reservations are based upon their inability to interpret their FRET experiments on linear DNA duplexes in terms of eq A2. They have assumed in their analysis of the duplex structures that the distance between D and A is directly proportional to the length of the DNA helix, an assumption which is probably not valid, due to the helical cylindrical structure of DNA. In similar experiments on varying length duplex DNA molecules using the experimental techniques discussed in the Appendix, we have obtained FRET efficiencies unequivocally in correspondence with Förster dipole–dipole transfer (manuscript in preparation). Similar FRET mea-

surements on nucleic acids will undoubtedly be very useful in the future. We feel that, provided the possible complexities are recognized and taken into account, there need be no unnecessary doubt or confusion that Förster dipole–dipole energy transfer is a useful tool to investigate stereochemical problems with DNA. FRET has been applied previously to study the structure of tRNA (Beardsley & Cantor, 1970) and has found wide application with other biomolecules (Stryer, 1978; Valeur, 1989). Many possible difficulties with FRET measurements (Cooper & Hagerman, 1990) can be circumvented, or possibly more effectively handled, using the type of analysis methods outlined in the Appendix.

In the Presence of Metal Ions the Four-Way Junctions Adopt a Well-Defined, Sequence-Specific Geometry. Neither the choice of stacking isomer (Murchie et al., 1989; this work) nor the ultimate extent of folding (this work) depend on the identity of the cation added. The free energy of folding of the junction appears to be determined largely by the favorable free energy of helix–helix stacking and the unfavorable electrostatic interactions in the folded structure. The former determines the isomeric form of the structure and should be largely unaffected by ions. The cations are required to reduce the latter. Two extreme roles for the metal ion in the folding process can be envisioned: (1) the ion plays the role of an active participant, becoming immobilized compared to its free state, or (2) the small ions have a more passive role, moderating the electrostatic repulsions arising from the close association of negatively charged groups while remaining mobile.

Do the ion titrations provide evidence to indicate which mode of ion association is responsible to enable the junction to fold into the stacked X form? We do not observe directly a complex containing a bound ion but rather a conformational change that is mediated by ion interactions with the macromolecule. The close proximity of the helical arms, especially at the point of strand exchange, makes the application of the common linear polyelectrolyte theories inapplicable, and perhaps we are guided best by only the simplest notions of ion complexes and polyelectrolytes. There is no indication to our knowledge that Na^+ is bound to DNA in an immobilized form as a molecular complex. And yet our ion titrations show that it is possible to fold the junction into a stacked X-form with Na^+. The ultimate extent of energy transfer in the fully folded junction (Figure 5) is the same for Mg^{2+}, Ca^{2+}, and Na^+. This seems to exclude that the folded junction creates a negatively charged phosphate pocket that *must* be occupied by an immobilized site-binding cation. However, a negative charge density of phosphates must certainly accumulate at the exchange point in the folded form, as indicated by the resistance to folding at lower ionic strengths and molecular modeling calculations of the folded junction (von Kitzing et al., 1990). This is further confirmed by experiments in which phosphate groups at the point of strand exchange were substituted by electrically neutral methyl phosphonates (Duckett et al., 1990); it was found that the junction isomerized so as to place the neutral phosphonate on the exchanging strands, suggesting that this is the point of maximum electrostatic repulsion.

According to the above arguments, it seems likely that an accumulation of negative charge upon folding the four-way junction can be compensated by an increased local charge density of highly mobile cations. The effective charge density of DNA is far below the linear density of phosphates, due to what is often referred to as an "atmosphere" of surrounding counterions; the density of counterions in the immediate vicinity of the polyelectrolyte are above the ion density in the solution far from the polyelectrolyte [≥80% of the counterions needed to neutralize fully the DNA charge in the solution have no measurable activity (Katchalsky, 1971; Manning, 1970)]. This apparent reduced charge on DNA changes only slightly with increasing ionic strength. However, increasing the ion concentration of the solvent does ensure a faster decrease of the negative electrostatic potential as a function of the distance from the phosphates (Daune, 1974; Katchalsky et al., 1966); this is due to an increase in the cation density close to the DNA negative charges. A graphic representation of local variations in charge density close to the surface of B-DNA (and Z-DNA) at 100 mM singly charged ion concentrations is shown in recent molecular model calculations by Klement et al. (1991). Such a local density of highly mobile positive charge has the effect of lowering the repulsion between phosphates, allowing them to approach each other more closely. Thus, even without site binding it is understandable how cations can act as an ion switch and assist the junction to fold in an ion concentration dependent manner. The ion concentration must be increased enough so that the negative charge density, inherent in the geometry of the folded junction, is compensated sufficiently.

Whether the final geometry of the folded junction (once it is electrostatically possible) is dictated mostly by forces other than those of electrostatic origin (stacking, van der Waals, steric constraints), or whether electrostatic forces play a major role in prescribing the feasible ensemble of possible folded structures, is not known. Model calculations indicate that the antiparallel stacked X-structure provides a fully stacked and folded molecular arrangement with less phosphate repulsion (and less steric repulsion) at the point of strand exchange than many other possibilities (von Kitzing et al., 1990). Perhaps this question can be resolved by varying solvent parameters or changing local structural and electronic aspects of the DNA and observing the conformational folding of the junction with energy transfer, as described here.

In summary, the proposed antiparallel stacked X-structure of the four-way genetic junction (Duckett et al., 1988; Murchie et al., 1989; von Kitzing et al., 1990) shown in Figure 6 accounts for the fluorescence energy transfer data determined by (1) increased acceptor steady-state emission measurements on three different junction sequences, (2) donor quantum yield decrease, and (3) donor fluorescence lifetimes. In the absence of added metal ions, the junction adopts a more extended structure. Ion titrations indicate (1) that the four-way junction folds to yield the same extent of energy transfer with Na^+, as with Mg^{2+} and Ca^{2+}, and therefore probably a closely similar molecular structure, (2) that the folding process from the low salt extended structure to the stacked X-structure occurs in a continuous noncooperative manner as the ion concentration is increased, similar to a simple bimolecular titration of the DNA with the ions, and (3) that the probable effect of the cations is to supply a sufficiently high local density of highly mobile positive charge around the phosphates to allow the compact structure of the junction to form.

We have used FRET to obtain useful information on the geometry and transitions in an important DNA structure. We expect that FRET will become more popular to investigate nucleic structures, just as this well-established technique has been usefully applied to numerous biological and polymeric systems (Stryer, 1978; Valeur, 1989).

Acknowledgments

We acknowledge with pleasure Drs. E. v. Kitzing for close collaboration on theoretical aspects of the four-way junction structure, T. M. Jovin and Karsten Rippe for general discussions and critical remarks on the manuscript, M. Soumpasis and R. Klement for discussions on DNA–ion interactions, and

G. Marriott for advice on the early fluorescence lifetime measurements.

APPENDIX

Steady-State and Time-Resolved FRET

The rate of energy transfer, k_T, from the singlet state of the donor D to the singlet state of the acceptor A is (Förster, 1949)

$$k_T = \left(\frac{R_0}{R}\right)^6 / \tau_D \qquad \text{(A1)}$$

where $R_0^6 = (8.785 \times 10^{-25})\Phi_D\kappa^2 n^{-4} J(\nu)$ cm^6, Φ_D and τ_D are the emission quantum yield and lifetime of D in the absence of A, $J(\nu)$ is the overlap integral, R is the scalar D–A separation, n is the index of refraction of the condensed matter between the D and A [$n = 1.4$ (Cantor & Tao, 1971)], and κ is the orientation factor for dipole–dipole coupling. Sufficient rotational freedom of just the donor can render κ^2 constant (Stryer, 1978); the fluorescence anisotropy of fluorescein is low enough so that we can make a reasonable approximation that κ^2 is constant for all samples. For a particular configuration of the donor and acceptor, the "efficiency of energy transfer" E is defined in terms of kinetic constants of decay from the excited state of the donor.

$$E = \frac{k_T}{\tau_D^{-1} + k_T} = \frac{1}{1 + (R/R_0)^6} \qquad \text{(A2)}$$

There may be several different configurations of D and A, each with possibly different values of R and R_0, in which case the observed efficiency is the appropriate average over the molecular ensemble.

From eq A2, the efficiency can be written in terms of the lifetimes

$$E = 1 - \frac{\tau_{DA}}{\tau_D} \quad \text{where} \quad \frac{1}{\tau_{DA}} = k_T + \frac{1}{\tau_D} \qquad \text{(A3)}$$

τ_{DA} is the lifetime of the donor in the presence of FRET.

The Efficiency of Energy Transfer Is Measured from the Induced Emission of the Acceptor as Follows (see Figure 2). (1) The fluorescein contribution from each energy transfer emission spectrum is removed by fitting the 500–530-nm portion (only fluorescein emits in this region) to a standard fluorescein spectrum (obtained from a singly labeled fluorescein junction) and subtracting this fluorescein emission component from the emission spectrum at every wavelength. The similarity between the fluorescein portion of the doubly labeled molecules and singly labeled fluorescein samples shows that the emission spectrum of fluorescein is not affected by the presence of rhodamine. (2) The resulting spectrum, consisting of only the rhodamine emission, is divided by the maximum (or the integrated intensity between 530 and 570 nm) of the excitation spectrum from the same sample (an emission spectrum excited at ~565 nm can also be used for this purpose). This normalizes the acceptor FRET signal for the quantum yield of rhodamine, for the concentration of the junction molecules, and for any error in the percent acceptor labeling. A comparison of this derived acceptor spectrum with the spectrum of a singly labeled rhodamine junction shows that there is no shift in the emission energies of the rhodamine in the doubly labeled molecules, indicating a lack of strong interaction between the DNA and the dye. The precision of the measurement is determined by measuring the repeatability of the quantities discussed below several times on certain junction vectors. Normalizing the fluorescence emission to the concentration of molecules is necessary for all FRET determinations. Achieving this with fluorescence spectral measurements on the samples alone has advantages (Conrad & Brand, 1968), especially when determining the acceptor emission. The following is a quantitative description of the formalism just described.

In the following, the superscripts D and A refer to the donor and acceptor. $\epsilon^D(\nu')$ is the molar absorption coefficient of the donor, $\Phi^D(\nu)$ is an emission spectrum shape function proportional to the fluorescence quantum yield of the donor, and $F^D(\nu,\nu')$ is the spectral component of the donor contributing to the total fluorescence emission spectrum. $\epsilon^A(\nu')$, $\Phi^A(\nu)$, and $F^A(\nu,\nu')$ are the corresponding parameters for the acceptor. $F^A(\nu,\nu')$ is derived from both direct excitation and energy transfer from the donor.

After subtracting the fluorescein spectral component from the fluorescence emission and dividing by the directly excited rhodamine signal, as described above, the following ratio is then formed:

$$(\text{ratio})_A = \frac{F'(\nu_1,\nu')}{F(\nu_2,\nu'')} \qquad \text{(A4)}$$

For 100% labeled molecules, this ratio can be shown to be

$$(\text{ratio})_A = \left[E\frac{\epsilon^D(\nu')}{\epsilon^A(\nu'')} + \frac{\epsilon^A(\nu')}{\epsilon^A(\nu'')}\right]\frac{\Phi^A(\nu_1)}{\Phi^A(\nu_2)} \qquad \text{(A5)}$$

$\epsilon^A(\nu')/\epsilon^A(\nu'')$ is known, and $\epsilon^D(\nu')/\epsilon^A(\nu'')$ can also be measured. Of course, all instrumentation constants resulting from differences between the settings of the instrument for the excitation and emission spectra must be taken into account (this is not shown explicitly in eq A5). For this work, $F'(\nu_1,\nu')$ is determined from an emission spectrum and $F(\nu_2,\nu'')$ from either an excitation or emission spectrum. The values given in the figures in this paper use excitation spectra. Measuring the enhanced fluorescence of the acceptor according to eq A3 avoids many experimental factors that could introduce uncertainty in the FRET measurement and normalizes the measurement to be independent of the concentrations of junction molecules.

The Efficiency of Transfer Can Also Be Determined by Measuring the Decrease in the Donor Quantum Yield. With the donor–acceptor pairs we are using, there are emission wavelengths where only donor emission is observed with no contribution from the acceptor; for instance, exciting at 490 nm and observing the emission between 500 and 530 nm, only fluorescein emission is observed.

We can normalize by the same acceptor fluorescence measurement as in eqs A3 and A4, to give the following ratio:

$$(\text{ratio})_D = \frac{F^D_{ex}(\nu_1,\nu')}{F^A_{ex}(\nu_2,\nu'')} = \frac{\epsilon^D(\nu')}{\epsilon^A(\nu'')}\frac{\Phi^D(\nu_1)}{\Phi^A(\nu_2)}(1 - E) \qquad \text{(A6)}$$

Equation A4 Shows How the Rate of Energy Transfer Can Be Determined Directly from Measurements of the Fluorescence Lifetime. The fluorescence lifetime of the donor–acceptor complex is measured at an emission wavelength where only donor emission is present (518 nm for fluorescein). The lifetime of fluorescein is 3–4 ns, and our measurement has a precision of ~100 ps. If $R_0 = 50$ Å, we should observe a 400–600-ps decrease in the donor (fluorescein) lifetime if the angle between neighboring labeled arms is ~60°, compared to two maximally extended arms. Exceptionally accurate measurements of the fluorescence lifetimes would be required to determine an accurate distance. But consistent global differences within the junction series between doubly labeled junctions are observable (see Results).

Analysis of the Ion Titrations

An additional analysis is required in order to use energy transfer measurements to monitor the folding reaction during the ion titrations since the quantum yields of the conjugated fluorescein and rhodamine junctions are functions of the ionic strength. Φ^D is a linear term in the expression for $(R_0)^6$ (see sentence following eq A1), and this will affect E. Φ^D is strongly dependent upon the salt concentrations (Figure 5). An ion titration of a junction singly labeled with fluorescein must be made in order to take the change in Φ^D into account in the fitting process. E is small for the junction molecules presented here; therefore, $E \approx (R_0/R)^6$. The portion of the ratio signal due to the energy transfer is corrected at every ion concentration by multiplying the first term of eq A5 by a ratio of the singly labeled junction fluorescence without added salt to the fluorescence of the singly labeled junction with the added salt. The resulting corrected energy transfer ratio points are then fitted with a full quadratic expression of binary binding, taking the dilution of the solution into account (Loontiens et al., 1990). If E is too large, the ion dependence of Φ^D must be introduced into the function and the fitting process iterated.

Formal Thermodynamic Description of the Ion Binding

The description of alkali and alkaline earth metal ion interactions with single conformation of DNA is complex; here, in addition, we are observing a structural change that is induced by varying the ion concentrations. Our results show that the fraction of the junction concentration in the unfolded and folded state, f_u and f_f, is a function of the ion concentration and that these fractional values, at any ionic strength, depend upon the type of small ions present. There are two general representations of this structural change as a reaction: (1) a simple conformational change of the junction molecules, $J_u \leftrightarrow J_f$, or (2) as a binding reaction between the cation and the junction molecule, N_c(cation) + $J_u \leftrightarrow J_f$ (N_c is the number of ions participating in the reaction). The formal equivalence between cases 1 and 2 has been discussed (Soumpasis & Jovin, 1987). It is not necessary that the actual molecular mechanism involve a site-specific bimolecular complex as depicted by the formal binding reaction of case 2, but this portrayal does provide a convenient representation to analyze the ion titrations. For the case 2, a bimolecular reaction (i.e., $N_c = 1$) accounts for our titration data. This indicates that there is no cooperative unit involved in the folding conformational change of the four-way junction, contrary to many other DNA structural transitions that extend over many base pairs, such as the cooperative reaction from B- to Z-DNA (Soumpasis & Jovin, 1987).

Stern–Volmer Plot

The slope of a Stern–Volmer plot for dynamic quenching is equal to $k_q\tau_0$, where τ_0 is the fluorescence lifetime in the absence of external quencher and the diffusion-controlled bimolecular rate constant $k_q = \gamma 4\pi RDN/1000$, R = the collision radius, $D = (D_f + D_q)$, where D_f and D_q are the diffusion constants of the fluorophore and the quencher [in our case $D \sim kT/(6\pi\eta R)$, k = Boltzmann's constant, and η is the viscosity], N = Avogadro's number, and γ = a quenching efficiency (number of effective collisions) including geometrical factors as well as efficiencies for free reaction species.

Registry No. Mg, 7439-95-4; Ca, 7440-70-2; Na, 7440-23-5.

REFERENCES

Beardsley, K., & Cantor, C. R. (1970) *Proc. Natl. Acad. Sci. U.S.A. 65*, 39.

Beaucage, S. L., & Caruthers, M. H. (1981) *Tetrahedron Lett. 22*, 1859–1862.

Bhattacharyya, A., Murchie, A. I. H., von Kitzing, E., Diekmann, S., Kemper, B., & Lilley, D. M. J. (1991) *J. Mol. Biol. 221*, 1191–1207.

Calascibetta, F. G., de Santis, P., Morosetti, S., Palleschi, A., & Savino, M. (1984) *Gazz. Chim. Ital. 114*, 437–441.

Cantor, C. R. & Tao, T. (1971) in *Proceedings in Nucleic Acid Research* (Cantoni, G. L., Ed.) pp 31–93, Harper & Row, New York.

Churchill, M. E., Tullius, T. D., Kallenbach, N. R., & Seeman, N. C. (1988) *Proc. Natl. Acad. Sci. U.S.A. 85*, 4653–4656.

Connolly, B. A. (1987) *Nucleic Acids Res. 15*, 3131–3139.

Conrad, R. H., & Brand, L. (1968) *Biochemistry 7*, 777–787.

Cooper, J. P., & Hagerman, P. J. (1987) *J. Mol. Biol. 198*, 711–719.

Cooper, J. P., & Hagerman, P. J. (1989) *Proc. Natl. Acad. Sci. U.S.A. 85*, 4653–4656.

Cooper, J. P., & Hagerman, P. J. (1990) *Biochemistry 29*, 9261–9268.

Daune, M. (1974) in *Metal Ions in Biological Systems* (Sigel, H., Ed.) pp 1–43, Marcel Dekker, Inc., New York.

De Boeck, H., MacGregor, R. B. J., Clegg, R. M., Sharon, N., & Loontiens, F. G. (1985) *Eur. J. Biochem. 149*, 141.

Duckett, D. R., Murchie, A. I. H., Diekmann, S., von Kitzing, E., Kemper, B., & Lilley, D. M. J. (1988) *Cell 55*, 79–89.

Duckett, D. R., Murchie, A. I. H., & Lilley, D. M. J. (1990) *EMBO J. 9*, 583–590.

Förster, T. (1949) *Z. Naturforsch. 4a*, 321–327.

Förster, T. (1951) *Fluoreszenz Organischer Verbindungen*, Vandenhoeck & Ruprecht, Göttingen.

Gough, G. W., & Lilley, D. M. J. (1985) *Nature 313*, 154–156.

Gratton, E., & Limkeman, M. (1983) *Biophys. J. 44*, 315.

Haugland, R. P. (1989) in *Optical Microscopy for Biology* (Herman, B. a. J., K., Ed.) pp 143–157, Wiley-Liss, New York.

Holliday, R. (1964) *Genet. Res. 5*, 282–304.

Katchalsky, A. (1971) *Pure Appl. Chem. 26*, 327–374.

Katchalsky, A., Alexandrowicz, Z., & Kedem, O. (1966) in *Chemical Physics of Ionic Solutions* (Conway, B. E. & Barradas, R. G., Eds.) pp 295–346, John Wiley & Sons, Inc., New York.

Klement, R., Soumpasis, D. M., & Jovin, T. M. (1991) *Proc. Natl. Acad. Sci. U.S.A. 88*, 4631–4635.

Loontiens, F. G., Regenfuss, P., Zechel, A., Dumortier, D., & Clegg, R. M. (1990) *Biochemistry 29*, 9029–9039.

Lu, M., Guo, Q., Seeman, N. C., & Kallenbach, N. R. (1989) *J. Biol. Chem. 264*, 20851–20854.

Manning, G. S. (1970) *Q. Rev. Biophys. 11*, 179–246.

Meselson, M. S., & Radding, C. M. (1975) *Proc. Natl. Acad. Sci. U.S.A. 72*, 358–361.

Murchie, A. I. H., Clegg, R. M., von Kitzing, E., Duckett, D. R., Diekmann, S., & Lilley, D. M. J. (1989) *Nature 341*, 763–766.

Murchie, A. I. H., Carter, W. A., Portugal, J., & Lilley, D. M. J. (1990) *Nucleic Acids Res. 18*, 2599–2606.

Murchie, A. I. H., Portugal, J., & Lilley, D. M. J. (1991) *EMBO J. 10*, 713–718.

Nickel, B. (1989) *J. Lumin. 44*, 1–18.

Orr-Weaver, T. L., Szostak, J. W., & Rothstein, R. J. (1981) *Proc. Natl. Acad. Sci. U.S.A. 78*, 6354–6358.

Piston, D. W., Marriott, G., Radivoyevich, T., Clegg, R. M., Jovin, T. M., & Gratton, E. (1989) *Rev. Sci. Instrum. 60*, 2596–2600.

Sigal, N., & Alberts, B. (1972) *J. Mol. Biol. 71*, 789–793.

Sinha, N. D., Biernat, J., McManus, J., & Koster, H. (1984) *Nucleic Acids Res. 12*, 4539-4557.
Sobell, H. M. (1972) *Proc. Natl. Acad. Sci. U.S.A. 69*, 2483-2487.
Soumpasis, D. M., & Jovin, T. M. (1987) in *Nucleic Acids and Molecular Biology* (Eckstein, F., & Lilley, D. M. J., Eds.) pp 85-111, Springer-Verlag, Berlin Heidelberg.
Spencer, R. D., & Weber, G. (1969) *Ann. Acad. Sci. Fenn., Ser. A2 158*, 361.
Steinberg, I. Z. (1968) *J. Chem. Phys. 48*, 2411-2413.
Stryer, L. (1978) *Annu. Rev. Biochem. 47*, 819-846.
Timsit, Y., Westhof, E., Fuchs, R. P. P., & Moras, D. (1989) *Nature 341*, 459-462.
Valeur, B. (1989) in *Fluorescent Biomolecules: Methodologies and Applications* (Reinhart, D. M. J. a. G. D., Ed.) pp 269-303, Plenum Press, New York.
von Kitzing, E., Lilley, D. M. J., & Diekmann, S. (1990) *Nucleic Acids Res. 18*, 2671-2683.

Backbone Dynamics of Calcium-Loaded Calbindin D_{9k} Studied by Two-Dimensional Proton-Detected ^{15}N NMR Spectroscopy†

Johan Kördel,‡ Nicholas J. Skelton, Mikael Akke,‡ Arthur G. Palmer, III,* and Walter J. Chazin*
Department of Molecular Biology, The Scripps Research Institute, La Jolla, California 92037
Received December 16, 1991; Revised Manuscript Received March 11, 1992

ABSTRACT: Backbone dynamics of calcium-loaded calbindin D_{9k} have been investigated by two-dimensional proton-detected heteronuclear nuclear magnetic resonance spectroscopy, using a uniformly ^{15}N enriched protein sample. Spin–lattice relaxation rate constants, spin–spin relaxation rate constants, and steady-state $\{^1H\}$–^{15}N nuclear Overhauser effects were determined for 71 of the 72 backbone amide ^{15}N nuclei. The relaxation parameters were analyzed using a model-free formalism that incorporates the overall rotational correlation time of the molecule, and a generalized order parameter (S^2) and an effective internal correlation time for each amide group. Calbindin D_{9k} contains two helix–loop–helix motifs joined by a linker loop at one end of the protein and a β-type interaction between the two calcium-binding loops at the other end. The amplitude of motions for the calcium-binding loops and the helices are similar, as judged from the average S^2 values of 0.83 ± 0.05 and 0.85 ± 0.04, respectively. The linker region joining the two calcium-binding subdomains of the molecule has a significantly higher flexibility, as indicated by a substantially lower average S^2 value of 0.59 ± 0.23. For residues in the linker loop and at the C-terminus, the order parameter is further decomposed into separate order parameters for motional processes on two distinct time scales. The effective correlation times are significantly longer for helices I and IV than for helices II and III or for the calcium-binding loops. Residue by residue comparisons reveal correlations of the order parameters with both the crystallographic *B*-factors and amide proton exchange rates, despite vast differences in the time scales to which these properties are sensitive. The order parameters are also utilized to distinguish regions of the NMR-derived three-dimensional structure of calbindin D_{9k} that are poorly defined due to inherently high flexibility, from poorly defined regions with average flexibility but a low density of structural constraints.

Calbindin D_{9k} is a small calcium-binding protein structurally homologous to the globular domains of calmodulin (CaM)[1] and troponin C (TnC). These proteins belong to the superfamily of proteins that bind Ca^{2+} ions through a common structural motif consisting of a calcium-binding loop flanked by two helices, termed the EF-hand (Kretsinger, 1987). The EF-hands generally occur in pairs, with a parallel arrangement as detailed in Figure 1. Cooperativity in the binding of calcium has been observed for some members of the CaM superfamily and has been attributed to the β-type interaction between the two calcium-binding loops (Seamon & Kretsinger, 1983; Linse et al., 1987). The binding of Ca^{2+} ions has been proposed to result in substantial structural rearrangements of the helices (Herzberg et al., 1986), which changes the nature of the interactions of these proteins with their target molecules. The proposed structural rearrangements provide a molecular mechanism for the activation of CaM [for a review, see Manalan and Klee (1984)] and TnC (Potter & Johnson, 1982). The best available model for structural rearrangements upon calcium binding is based on a comparison of the (apo) N-terminal and (Ca^{2+}-loaded) C-terminal domains in the TnC crystal structure (Herzberg et al., 1986). This model has not been directly verified or refined because none of the proteins in the calmodulin superfamily have been crystallized with *different* levels of calcium loading. Structure determination *in solution* by NMR circumvents the need for crystallization and therefore is being applied to determine the structural

† This work was supported by the National Institutes of Health (Grant GM 40120 to W.J.C.), The American Cancer Society (fellowship JFRA-294 to W.J.C.), the National Science Foundation (postdoctoral fellowship CHE-8907510 to A.G.P.), the Swedish Natural Science Research Council (graduate fellowships to J.K. and M.A.), and the Royal Swedish Academy of Sciences (travel grant to J.K.).
* To whom correspondence should be addressed.
‡ Permanent address: Department of Physical Chemistry 2, Chemical Centre, University of Lund, S-221 00 Lund, Sweden.

[1] Abbreviations: P43G, recombinant bovine calbindin D_{9k} mutant with Pro43 substituted by glycine; CaM, calmodulin; TnC, troponin C; NMR, nuclear magnetic resonance; 2D, two-dimensional; NOE, nuclear Overhauser effect; NOESY, two-dimensional NOE spectroscopy; R_1, spin–lattice or longitudinal relaxation rate constant; R_2, spin–spin or transverse relaxation rate constant; CSA, chemical shift anisotropy; INEPT, insensitive nuclei enhanced by polarization transfer; CPMG, Carr–Purcell–Meiboom–Gill; TPPI, time-proportional phase incrementation; FID, free induction decay; RMS, root mean square; ANOVA, analysis of variance.

0006-2960/92/0431-4856$03.00/0